Supplementary Information

Multiplex Three-Dimensional Mapping of Macromolecular Drug Distribution in the Tumor Microenvironment

Steve Seung-Young Lee, Vytautas P. Bindokas, Stephen J. Kron

Correspondence to Stephen J. Kron
Email: skron@uchicago.edu

This PDF file includes:

Supplementary tables S1-2
Supplementary figures S1-6
Captions for supplementary videos 1 to 7

Other supplementary materials for this manuscript include the following:

Supplementary videos 1-7

Supplementary Table S1. Fluorescent antibody conjugation

Antibody	Clone	Source	Antibody Concentration	Fluorescent Dye	Added Dye*
Anti-rat Her2	7.16.4		0.6 mg/0.5 ml	DyLight™ 488 NHS ester	140 µg
			1 mg/0.5 ml (*i.v.*)	DyLight™ 594 NHS ester	70 µg
Anti-reticular fibroblasts and fibres	ER-TR7	BioXCell	1 mg/1 ml	DyLight™ 680 NHS ester	200 µg
Anti-CD8	2.43	BioXCell	0.5 mg/0.5 ml	DyLight™ 550 NHS ester	100 µg
Anti-SMA	1A4	Sigma-Aldrich	0.1 mg/0.1 ml	DyLight™ 488 NHS ester	20 µg
Anti-CD31	MEC13.3	Biolegend	0.5 mg/1 ml	DyLight™ 633 NHS ester	75 µg
Anti-EGFR	528	BioXCell	1 mg/0.5 ml (*i.v.*)	DyLight™ 594 NHS ester	70 µg
IgG Isotype	C1.18.4	BioXCell	1 mg/0.5 ml (*i.v.*)	DyLight™ 680 NHS ester	70 µg
Anti-PD-L1	10F.9G2	BioXCell	1 mg/0.5 ml (*i.v.*)	DyLight™ 594 NHS ester	70 µg
			0.4 mg/0.2 ml	DyLight™ 680 NHS ester	70 µg

*10 mg/ml in dimethylformamide

(*i.v.*) Intravenous injection for distribution study

Supplementary Table S2. Fiji macros for 3D image processing and analysis

Macro	Function
LIFtile-restitcher	align and stitch 3D mosaics for multi-channel images (0-999 image tiles)
HPRstack2ConstantMean	compensate for depth-related intensity losses
composite big aligner	automate alignment and registration of the stitched macrosection images
closeZvoids	merged top slice and bottom slice of the macrosections
hyprBKGDfix	clear background around tumor and tissue
vessel extractor	automate segmentation of the blood vessels

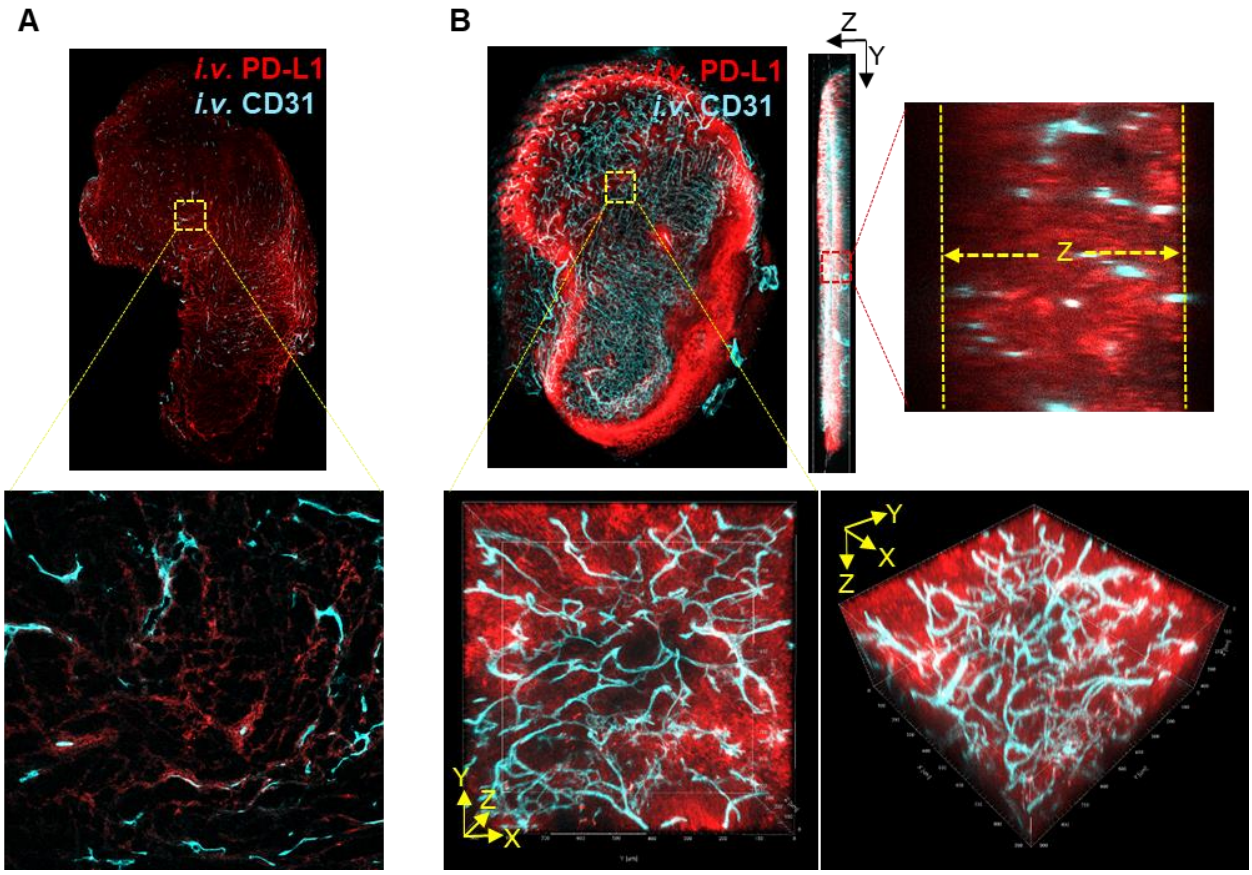

Supplementary Figure S1. Comparison of 2D and 3D images of anti-PD-L1 antibody drug distribution in tumor at 12 h post injection. **A,** 2D survey (top) and magnified (bottom) images of anti-PD-L1 antibody drug (red) and blood vessels (cyan) in 10 µm thick cryosection obtained from a divided TUBO tumor. **B,** 3D survey (top), lateral (right), optical Z cross-section (far right), and magnified (bottom) images of a 400 µm macrosection obtained from the divided TUBO tumor.

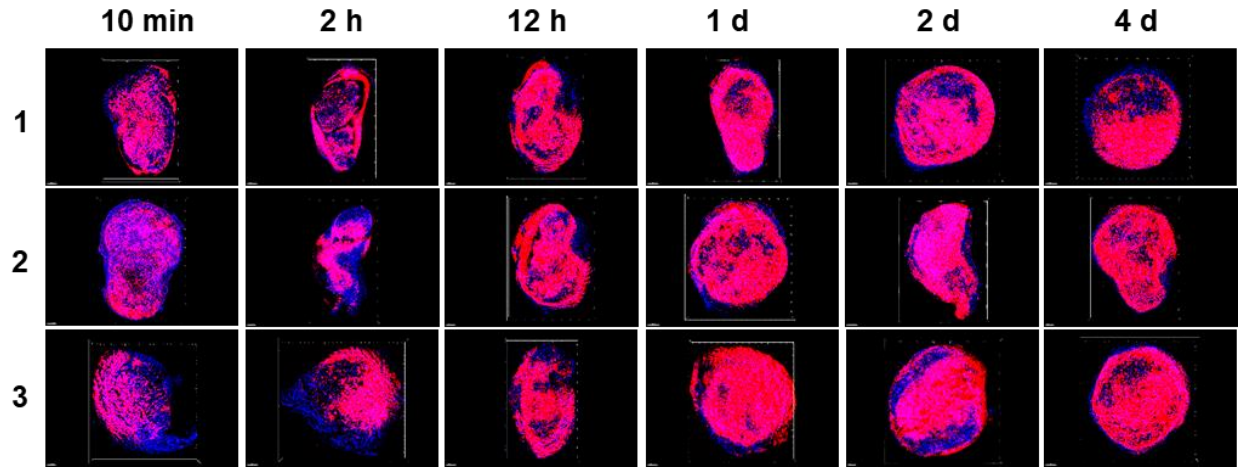

Supplementary Figure S2. 3D spatial pharmacokinetics of anti-PD-L1 antibody in tumor macrosections. Three macrosections from three different tumors for each time point were analyzed for determining 3D tumor penetration distance of anti-PD-L1 antibody drug (red) away from $CD31^+$ blood vessels (blue) in Fig. 2E and macrosection volume coverage (%) in Fig. 2F.

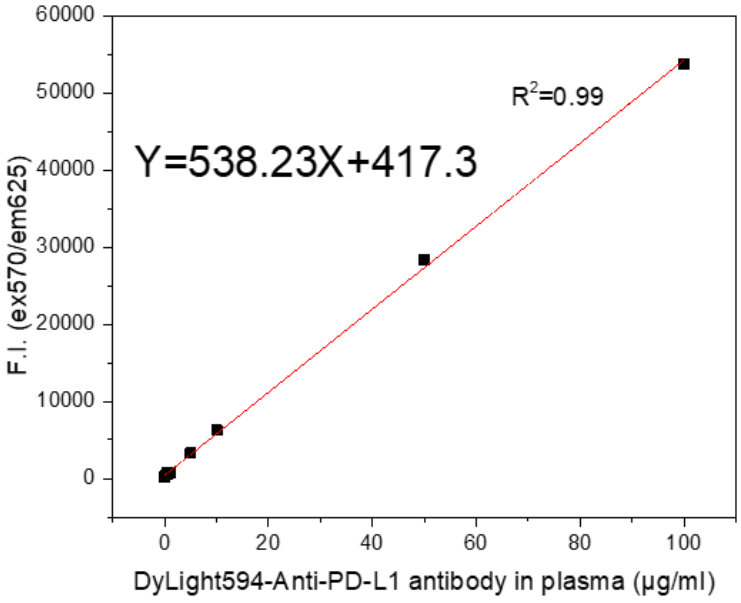

µg/ml	Fluorescence Intensity
100	54915.5
50	26909
10	6164.5
5	3390
1	760.5
0.5	613
0.1	327
0.05	249.5
0.01	171.5
0	159

Supplementary Figure S3. Fluorescence calibration curve for anti-PD-L1 antibody concentration in plasma. Fluorescence intensities (F.I.) of different concentrations of DyLight594-anti-PD-L1 (100-0.01 µg/ml) in plasma were measured at 570 nm excitation and 625 nm emission, and fitted to a linear equation.

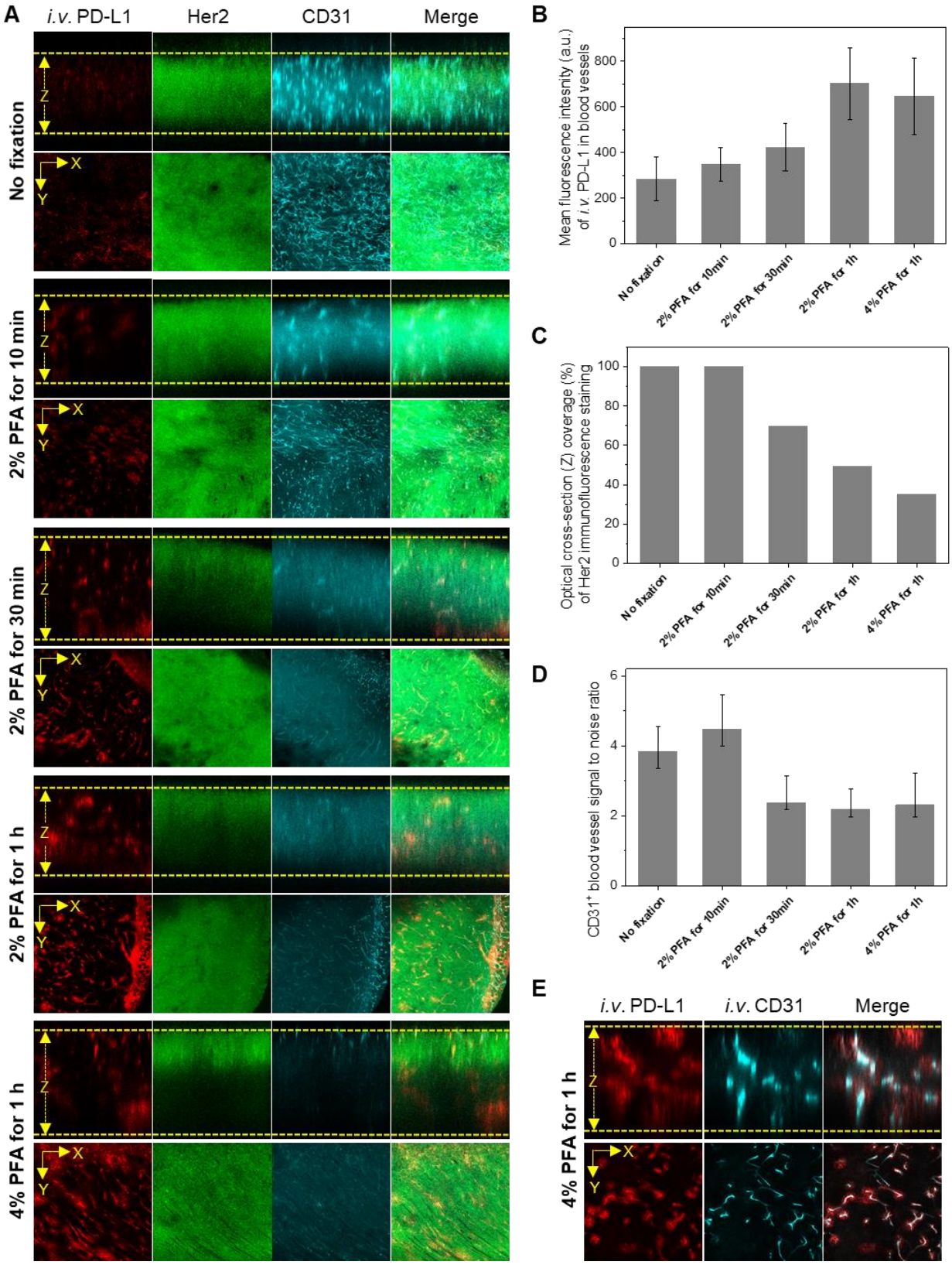
A
i.v. PD-L1
Her2
CD31
Merge
No fixation
2% PFA for 10 min
2% PFA for 30 min
2% PFA for 1 h
4% PFA for 1 h
Z
X
Y
B
Mean fluorescence intensity (a.u.) of i.v. PD-L1 in blood vessels
0
200
400
600
800
No fixation
2% PFA for 10min
2% PFA for 30min
2% PFA for 1h
4% PFA for 1h
C
Optical cross-section (Z) coverage (%) of Her2 immunofluorescence staining
0
20
40
60
80
100
No fixation
2% PFA for 10min
2% PFA for 30min
2% PFA for 1h
4% PFA for 1h
D
CD31+ blood vessel signal to noise ratio
0
2
4
6
No fixation
2% PFA for 10min
2% PFA for 30min
2% PFA for 1h
4% PFA for 1h
E
i.v. PD-L1
i.v. CD31
Merge
4% PFA for 1 h
Z
X
Y

Supplementary Figure S4. Optimizing fixation and immunostaining conditions for 3D imaging macromolecular drug distribution in 400 µm thick tumor macrosections. **A,** Optical cross-section (Z) scanning (top) and 2D imaging (bottom) of optically cleared tumor macrosections (400 µm thickness). Fluorescent anti-PD-L1 antibody (red) was intravenously (*i.v.*) injected into TUBO tumor bearing mice, and the tumors were excised at 10 min post injection of anti-PD-L1 antibody, fixed with paraformaldehyde (PFA) solution in different conditions, sectioned, and immunostained for $Her2^+$ cancer cells (green) and $CD31^+$ blood vessels (cyan). **B,** Relative quantification of fluorescence intensity of anti-PD-L1 antibody localized in $CD31^+$ blood vessels in the 2D images of macrosections fixed in the different conditions (n=9, three random 2D areas in three different macrosections, mean ± SD). **C,** Relative quantification of anti-Her2 antibody immunostaining efficiency for the macrosections fixed in different conditions. The coverage (%) of thresholded Her2 stained area in the optical cross-section (Z) scanning images as shown in A. **D,** Relative quantification of the signal-to-noise ratio of CD31-stained blood vessels in the 2D optical section images (n=9, three random 2D areas in three different macrosections, mean ± SD). **E,** Optical cross-section (Z) scanning (top) and 2D imaging (bottom) of an optically cleared macrosection that was derived from the tumor *in vivo* labeled for blood vessels by intravenous (*i.v.*) injection of fluorescent anti-CD31 antibody and fixed with 4% paraformaldehyde (PFA) solution for 1 h. The signal-to-noise ratio of CD31-positive blood vessels was 9.95.

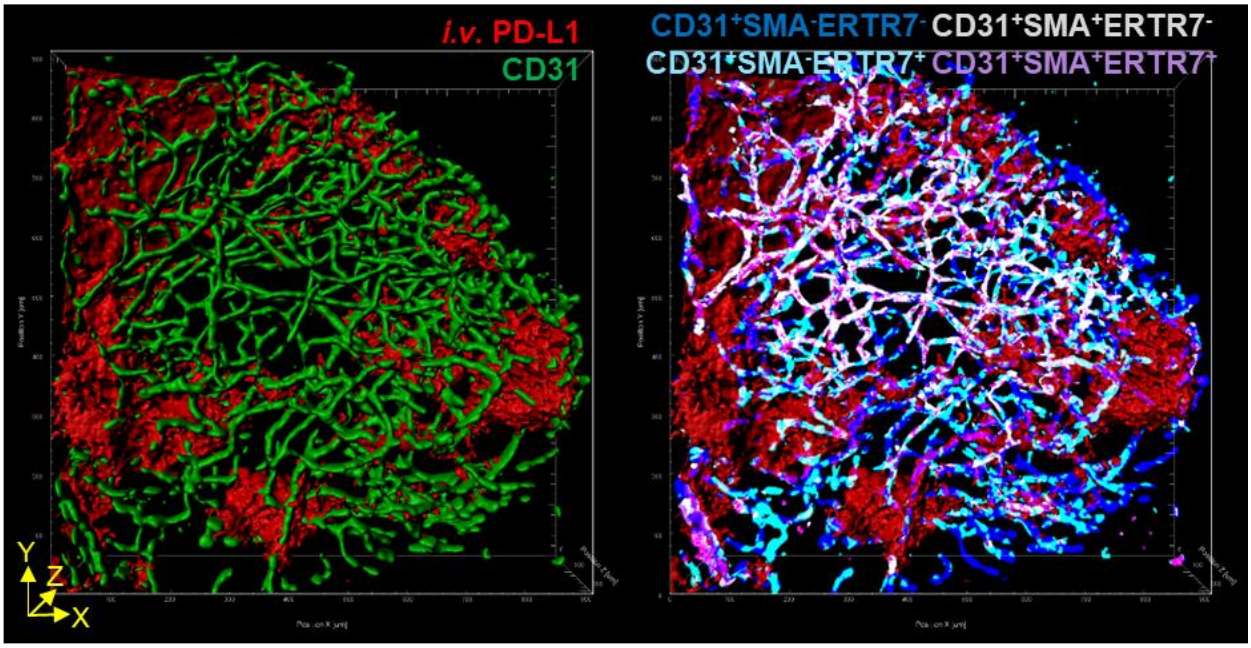

Supplementary Figure S5. 3D mapping of different types of microvessels and their permeability with regards to anti-PD-L1 antibody drug penetration into tumor.

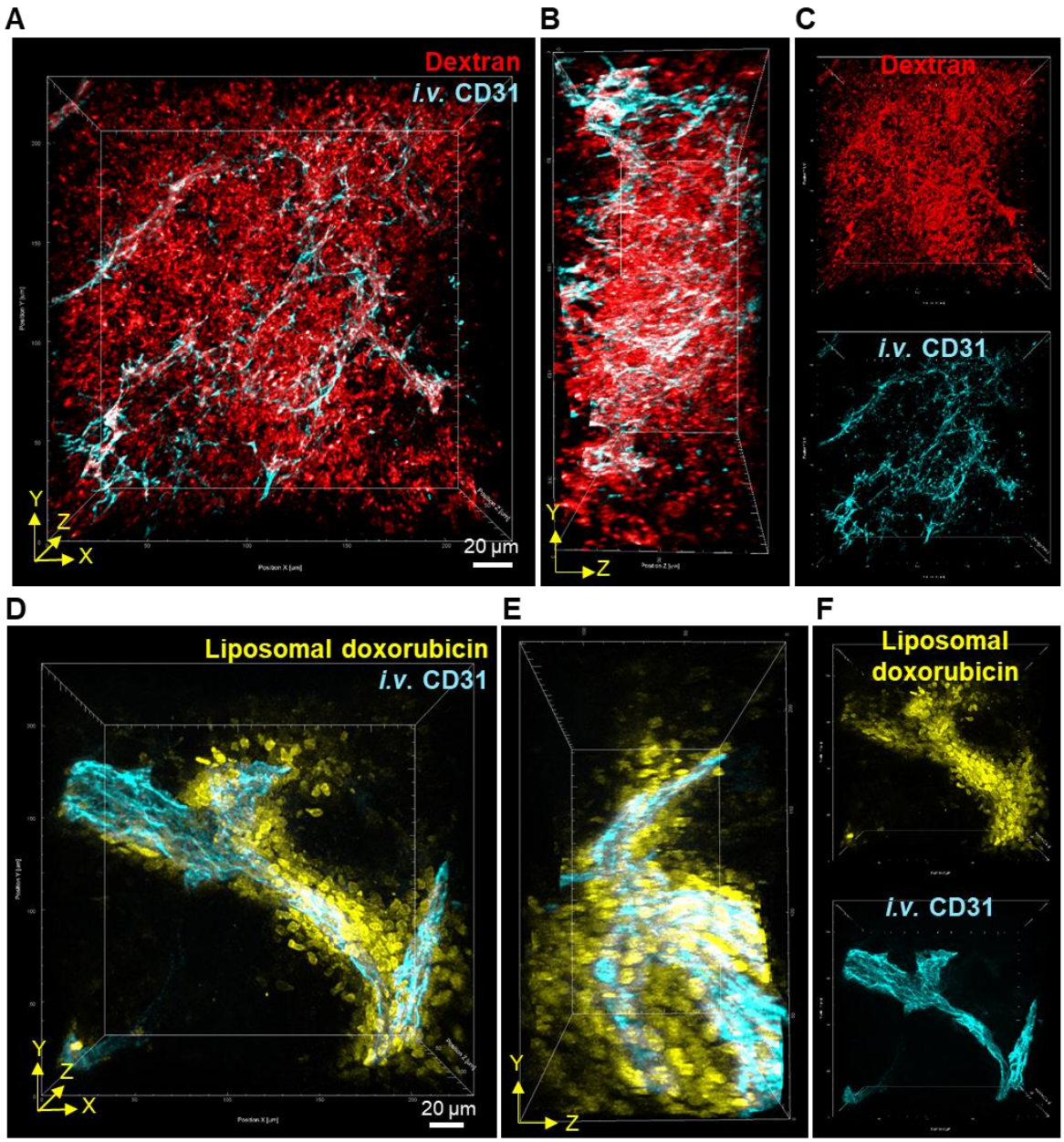

Supplementary Figure S6. 3D visualization of macromolecular drug distribution in tumors. **A, D,** High resolution 3D images of dextran (red) and doxorubicin (yellow)-loaded liposome (Doxil) distribution in mouse 4T1 tumors at 30 min and 4 h post injection, respectively. The tumor blood vessels (cyan) were *in vivo* labeled by intravenous (*i.v.*) injection of fluorescent anti-CD31 antibody. Scale bar: 20 µm. **B, E,** Lateral view of the 3D images and **C, F,** channel images for macromolecular drugs and tumor blood vessels.

Captions for supplementary videos 1 to 7

Supplementary Video 1. Tomographic visualization of anti-PD-L1 antibody drug distribution in reconstructed TUBO tumor image with multiple orthogonal planes. *i.v.* PD-L1 (red) and *i.v.* CD31 (cyan).

Supplementary Video 2. High resolution 3D rendering of vascular penetration of anti-PD-L1 antibody drug in TUBO tumor. *i.v.* PD-L1 (red) and *i.v.* CD31 (cyan).

Supplementary Video 3. 3D rendering of anti-PD-L1 antibody distribution in the tumor microenvironment at 10 min after injection. Her2 (green), CD8 (yellow), *i.v.* PD-L1 (red), CD31 (cyan), and PD-L1 (magenta).

Supplementary Video 4. 3D rendering of different types of microvessels and their permeability with regards to anti-PD-L1 antibody drug penetration into tumor. SMA (green), CD31 (cyan), ER-TR7 (magenta), and *i.v.* PD-L1 (red).

Supplementary Video 5. 3D rendering of anti-Her2 and IgG isotype antibody distribution in the BALB-NeuT tumor nest at 1 h after injection. *i.v.* Her2 (green), *i.v.* IgG (red), and *i.v.* CD31 (cyan).

Supplementary Video 6. 3D rendering of anti-EGFR and IgG isotype antibody distribution in the lung cancer PDX tumor nest at 1 h after injection. *i.v.* EGFR (green), *i.v.* IgG (red), and *i.v.* CD31 (cyan).

Supplementary Video 7. 3D rendering of doxorubicin delivery to tumor in mouse treated with PEGylated liposomal doxorubicin (Doxil), showing cell uptake at 4 h after injection. Doxorubicin bound to nuclear DNA (yellow) and *i.v.* CD31 (cyan).